Validation of stratospheric nitric acid profiles observed by Improved Limb Atmospheric Spectrometer (ILAS)–II

H. Irie,[1] T. Sugita,[2] H. Nakajima,[2] T. Yokota,[2] H. Oelhaf,[3] G. Wetzel,[3] G. C. Toon,[4] B. Sen,[4] M. L. Santee,[4] Y. Terao,[5] N. Saitoh,[2] M. K. Ejiri,[2] T. Tanaka,[2] Y. Kondo,[6] H. Kanzawa,[7] H. Kobayashi,[8] and Y. Sasano[2]

Received 22 April 2005; revised 13 September 2005; accepted 20 October 2005; published 29 March 2006.

[1] The Improved Limb Atmospheric Spectrometer-II (ILAS-II) was launched aboard the Advanced Earth Observing Satellite-II (ADEOS-II) in December 2002. Stratospheric vertical profiles of nitric acid (HNO_3) concentration observed by ILAS-II (version 1.4) are validated using coincident HNO_3 measurements by balloon-borne instruments (MIPAS-B2 and MkIV) in March and April 2003. Further validation is performed by making climatological comparisons of lower stratospheric HNO_3-ozone (O_3) correlations obtained by ILAS-II and ILAS (the predecessor of ILAS-II) for specific potential vorticity-based equivalent latitudes and seasons where and when ILAS data showed very compact correlations in 1997. The reduced scatter of ILAS-II HNO_3 values around the reference HNO_3, which is derived from ILAS-II O_3 using the ILAS HNO_3-O_3 correlation, shows that the precision of the ILAS-II HNO_3 data is better than 13–14%, 5%, and 1% at 15, 20, and 25 km, respectively. Combining all of the comparisons made in the present study, the accuracy of the ILAS-II HNO_3 profiles at 15–25 km is estimated to be better than −13%/+26%.

Citation: Irie, H., et al. (2006), Validation of stratospheric nitric acid profiles observed by Improved Limb Atmospheric Spectrometer (ILAS)–II, *J. Geophys. Res.*, *111*, D11S03, doi:10.1029/2005JD006115.

1. Introduction

[2] Polar stratospheric clouds (PSCs) play a central role in stratospheric ozone depletion over the Antarctic and Arctic in the winter/spring seasons. Nitric acid (HNO_3) is a key component determining the chemical and physical properties of PSCs that form at low temperatures ($<\sim$200 K) through condensation of HNO_3 and water vapor (H_2O) in the winter/spring polar stratosphere. Satellite measurements of HNO_3 concentrations have been widely used to investigate not only spatial distributions and temporal variations of HNO_3 [*Santee et al.*, 1995, 1997, 1998, 1999, 2000, 2004; *Irie et al.*, 2001] but also important details of the processes controlling stratospheric HNO_3 concentrations, e.g., the formation of PSC particles and denitrification [*Santee et al.*, 1998, 2002; *Hayashida et al.*, 2000; *Kondo et al.*, 2000a; *Irie et al.*, 2001, 2004; *Saitoh et al.*, 2002; *Irie and Kondo*, 2003; *Rivière et al.*, 2003]. While these processes are not fully understood, the Improved Limb Atmospheric Spectrometer-II (ILAS-II) onboard the Advanced Earth Observing Satellite-II (ADEOS-II) provided recent measurements of vertical profiles of HNO_3 concentration at high latitudes in both the Northern Hemisphere (NH) and the Southern Hemisphere (SH). Preoperational and operational observations by ILAS-II were performed in January–March and April–October 2003, respectively. In this paper, we assess the validity of the ILAS-II HNO_3 profiles retrieved with the version 1.4 algorithm under PSC-free conditions by using comparisons with HNO_3 profiles measured by balloon-borne instruments. Further assessment is performed from a climatological standpoint by comparing the lower stratospheric correlations between HNO_3 and ozone (O_3) mixing ratios obtained by ILAS-II in 2003 with those by ILAS (the predecessor of ILAS-II) in 1997. We choose O_3 as a companion species, because it can generally be validated more precisely than other species because of extensive ozonesonde and satellite O_3 data. We assume that HNO_3-O_3 correlations between 1997 and 2003 were invariant for the same latitudes and seasons. This assumption is supported from the multiyear data obtained by the Microwave

[1]Frontier Research Center for Global Change, Japan Agency for Marine-Earth Science and Technology, Yokohama, Japan.
[2]National Institute for Environmental Studies, Tsukuba, Japan.
[3]Institut für Meteorologie und Klimaforschung, Forschungszentrum Karlsruhe, Karlsruhe, Germany.
[4]Jet Propulsion Laboratory, California Institute of Technology, Pasadena, California, USA.
[5]Division of Engineering and Applied Sciences, Harvard University, Cambridge, Massachusetts, USA.
[6]Research Center for Advanced Science and Technology, University of Tokyo, Tokyo, Japan.
[7]Department of Earth and Environmental Sciences, Graduate School of Environmental Studies, Nagoya University, Nagoya, Japan.
[8]Central Research Institute of Electric Power Industry, Tokyo, Japan.

Copyright 2006 by the American Geophysical Union.
0148-0227/06/2005JD006115$09.00

Table 1. Repeatability Errors (%) for HNO_3 and O_3

Species	Hemisphere	15 km	20 km	25 km
HNO_3	NH	23	5	1
HNO_3	SH	17	5	3
O_3	NH	14	4	6
O_3	SH	11	5	2

Limb Sounder (MLS) onboard the Upper Atmosphere Research Satellite (UARS).

2. ILAS-II Measurements

2.1. Instrument

[3] The ILAS-II instrument, designed similarly to its predecessor ILAS [*Sasano et al.*, 1999], is a solar occultation sensor to measure stratospheric vertical profiles of various constituents, including HNO_3 and O_3. The ILAS-II instrument consists of infrared (channel 1, 6.2–11.8 μm), midinfrared (channel 2, 3.0–5.7 μm), narrow-band (channel 3, 12.78–12.85 μm), and visible (753–784 nm) spectrometers, and a sun edge sensor. The ILAS-II was launched aboard the ADEOS-II satellite on 14 December 2002, and performed about 400 preoperational observations between January and March 2003. The operational observations were made with a frequency of about 14 times per day in each hemisphere for about 7 months from 2 April through 24 October 2003. The measurement latitudes ranged from 54° to 71°N and from 65° to 88°S, varying seasonally with the geometric relationship between the Sun, the Earth, and the satellite.

2.2. Version 1.4 Retrieval Algorithm

[4] The version 1.4 retrieval algorithm was used to obtain gas concentration profiles from the absorption lines measured with the channel-1 infrared spectrometer (T. Yokota et al., unpublished manuscript, 2006). The algorithm primarily used the strong absorption lines around 7.6 and 11.3 μm for the HNO_3 retrieval and around 9.5–10.0 μm for O_3. Spectroscopic data were adopted from the year 2000 edition of the High-Resolution Transmission (HITRAN) database, including updates through the end of 2001 [*Rothman et al.*, 2003]. The HNO_3 and O_3 concentrations were retrieved simultaneously with other gases using a nonlinear least squares method [*Yokota et al.*, 2002], after estimating the contribution of aerosol attenuation at 7.12, 8.27, 10.60, and 11.76 μm, where contributions of gas absorption are relatively much smaller as compared to the other wavelength regions. These four spectral elements are called "window elements." The extinction coefficients of aerosols at the window elements were linearly interpolated and extrapolated with wave number to obtain transmittance due only to gaseous absorption over the whole range of infrared regions measured. This simple linear approximation may cause systematic errors in the HNO_3 and O_3 concentrations retrieved, as described below. Vertical profiles of concentration were retrieved by the so-called onion-peeling method [*Yokota et al.*, 2002], with vertical resolutions of 1.3–2.9 km at tangent heights of 15–55 km. The tangent heights of the measurements were determined with a sun edge sensor method and a transmittance spectrum method for altitudes above and below 30 km, respectively (for more details see *Nakajima et al.* [2002], T. Tanaka et al. (unpublished manuscript, 2006), and http://www-ilas2.nies.go.jp/en/).

2.3. Errors

[5] To evaluate the precision of the ILAS-II concentration data, for every series of 100 occultation measurements (corresponding to about an 8-day time period) we calculated an average and a 1σ standard deviation of the retrieved concentration data at each 1-km altitude for each hemisphere. The minimum of the ratio (1σ standard deviation)/(average) for the whole of the ILAS-II measurement period gives an upper limit of the precision, because it should represent the precision of the data with the smallest contributions from the natural variability in the measurement period. The minimum value is referred to as the "repeatability error" for all of the ILAS-II version 1.4 data products. For HNO_3 and O_3, the repeatability errors are summarized in Table 1, showing that the estimated upper limits of the precision at 15–25 km are 1–23% and 2–14%, respectively. In addition to the repeatability error, the retrieved concentration data can further be affected by uncertainty in the gas concentrations assumed in the calculation of the aerosol attenuation contribution to the spectra at window elements, as mentioned in section 2.2, and by the uncertainty in temperature [*Yokota et al.*, 2002]. The additional error due to these uncertainties is referred to as the "external error." The median external errors calculated from all the ILAS-II data are listed in Table 2. In comparisons of HNO_3 profiles obtained by ILAS-II and balloon-borne instruments below, we use the term "total error," which is defined as the root-sum-square of the repeatability and external errors.

[6] It should be noted that in the version 1.4 retrieval algorithm, the uncertainty in line parameters has not been considered in the calculation of the total error. While this omission may lead to an underestimate of the total error, the present paper empirically estimates the precision, which should contain all of the random error components, including random errors in line parameters. If the line parameters used contain systematic errors, they would be taken into account in future versions of the ILAS-II retrieval algorithm by using updated line parameter data.

[7] In the present paper, we will attempt to estimate the accuracy of ILAS-II HNO_3 profiles. For O_3, *Sugita et al.* [2006] have made statistically robust comparisons with a large amount of ozonesonde and satellite data (SAGE II/III, HALOE, and POAM III). The comparisons showed that most ILAS-II O_3 profiles agreed with ozonesonde and satellite data to within 10% at 10–40 km.

[8] As described above, aerosol extinction at all the wavelengths measured with the channel-1 infrared spec-

Table 2. External Errors[a] (%) for HNO_3 and O_3

Species	Hemisphere	15 km	20 km	25 km
HNO_3	NH	10	3	2
HNO_3	SH	9	3	3
O_3	NH	9	4	2
O_3	SH	10	5	1

[a]Median values calculated from all the ILAS-II data.

Table 3. Systematic Biases of HNO_3 and O_3 Caused by Optically Thick PSCs (AEC = 10^{-3} km^{-1}) at 20 km

	ICE	NAT	STS[a] (a)	STS[a] (b)	STS[a] (c)	STS[a] (d)
r,[b] μm	10	0.5	0.5	0.5	0.5	0.5
σ[c]	1.5	1.5	1.5	1.5	1.5	1.5
HNO_3, wt%	· · ·	· · ·	37	15	3	0.5
H_2SO_4, wt%	· · ·	· · ·	5	33	47	60
HNO_3 bias, 10^8 cm^{-3}	2.4	−16.0	−0.09	1.2	2.0	2.0
HNO_3 bias,[d] ppbv	0.14	−0.96	−0.005	0.07	0.12	0.12
O_3 bias, 10^{12} cm^{-3}	1.2	0.15	0.005	0.23	0.25	0.22
O_3 bias,[d] ppmv	0.74	0.09	0.003	0.14	0.15	0.13

[a]Supercooled ternary solution of $HNO_3/H_2SO_4/H_2O$.
[b]Mode radius.
[c]Standard deviation of a lognormal size distribution.
[d]Mixing ratios were calculated assuming the typical air number density at 20 km [*Yokota et al.*, 2002; T. Yokota et al., unpublished manuscript, 2006].

trometer was simply estimated using a linear interpolation and extrapolation from the aerosol absorption at four window wavelengths. This simple technique sometimes yields a bias in the HNO_3 and O_3 concentration retrievals, depending on composition and volume of aerosols/PSCs that are present in air masses observed. Similar to the work of *Yokota et al.* [2002] for ILAS, we performed a theoretical simulation to quantify the magnitude of the HNO_3 and O_3 biases as a function of aerosol extinction coefficient (AEC) at 780 nm for several PSC compositions. As in the ILAS results, the biases of the ILAS-II HNO_3 and O_3 concentrations were both well correlated with AEC in the simulations. Table 3 summarizes PSC composition and size distribution parameters assumed in the simulations and the estimated biases of the HNO_3 and O_3 concentrations for AEC = 10^{-3} km^{-1}. AEC values less than 10^{-3} km^{-1} are considered to include typical PSC conditions, because about 95% of all the ILAS-II AEC values at 20 km over the Antarctic were less than 10^{-3} km^{-1} for the period between April (late fall) and October (early spring) 2003. For AEC values less than 10^{-3} km^{-1}, the largest positive bias was possible in the case of ice PSCs, but was less than 2.4×10^8 cm^{-3} (corresponding to about 0.14 ppbv HNO_3 at 20 km) for HNO_3 and less than 1.2×10^{12} cm^{-3} (about 0.74 ppmv O_3 at 20 km) for O_3. The negative bias in HNO_3 concentration could reach 16.0×10^8 cm^{-3} (about 0.96 ppbv HNO_3 at 20 km) in the case of nitric acid trihydrate (NAT), whereas no negative bias in O_3 due to the presence of PSCs is predicted in any of the cases considered here.

3. Comparison With Balloon-Borne Measurements

3.1. Approach

[9] The ILAS-II HNO_3 vertical profiles are first compared with those measured by two balloon-borne instruments: (1) the Michelson Interferometer for Passive Atmospheric Sounding-Balloon-borne version 2 (MIPAS-B2) instrument [*Oelhaf et al.*, 1996; *Friedl-Vallon et al.*, 2004], which is a cryogenic Fourier transform infrared (FTIR) spectrometer measuring thermal emission from the limb of the atmosphere, and (2) the MkIV instrument [*Toon*, 1991; *Sen et al.*, 1998], which is a solar occultation FTIR spectrometer. For both MIPAS-B2 and MkIV, the HNO_3 profile used in the present study was retrieved using the HITRAN2000 spectroscopic database as used in the ILAS-II version 1.4 algorithm. The accuracy and precision of these balloon-borne HNO_3 measurements at 20 km are about 10–12% and 5%, respectively (Table 4). Vertical resolutions estimated from the instantaneous fields of view of the instruments are about 1.2 and 2.0 km for MIPAS-B2 and MkIV, respectively. As used in previous ILAS HNO_3 validation studies by *Koike et al.* [2000] and *Irie et al.* [2002], these measurement characteristics are sufficient to validate HNO_3 measurements made by satellite-borne solar occultation sensors.

[10] The measurements by MIPAS-B2 and MkIV instruments were performed near Kiruna, Sweden (67.9°N, 21.1°E), during the night on 20 March 2003, and at sunrise on 1 April 2003, respectively. On 20 March 2003, ILAS-II measurements were made very close to the locations of the MIPAS-B2 measurements; the distance between the ILAS-II and MIPAS-B2 measurement locations at an altitude of 20 km was only about 100 km (Table 4). The time difference was only 6 hours at 20 km (Table 4). In addition, the potential vorticity (PV) difference, based on United Kingdom Met Office (UKMO) data, was only 4% at the potential temperature corresponding to the 20-km altitude of the MIPAS-B2 measurements. On the other hand, no ILAS-II measurement was made on 1 April 2003, when the MkIV measurement was made. However, forward isentropic trajectories calculated from the time and location of the MkIV measurements using UKMO wind fields (Figure 1)

Table 4. List of Balloon Measurements

Instrument	Date	Accuracy,[a] %	Precision,[a] %	Distance,[b] km	Time Difference,[b] hour	PV Difference,[c] %
MIPAS-B2	20 Mar.	10	5	104	5.8	4
MkIV	1 Apr.	12	5	2500 (518–585)[d]	33.6 (<1.0)[d]	1

[a]One-σ values at 20 km.
[b]Values between the ILAS-II and balloon measurement locations at 20 km.
[c]Values between the ILAS-II and balloon measurement locations at the same potential temperature level near 20 km.
[d]Values between the ILAS-II and MkIV air masses using trajectories at 20 km.

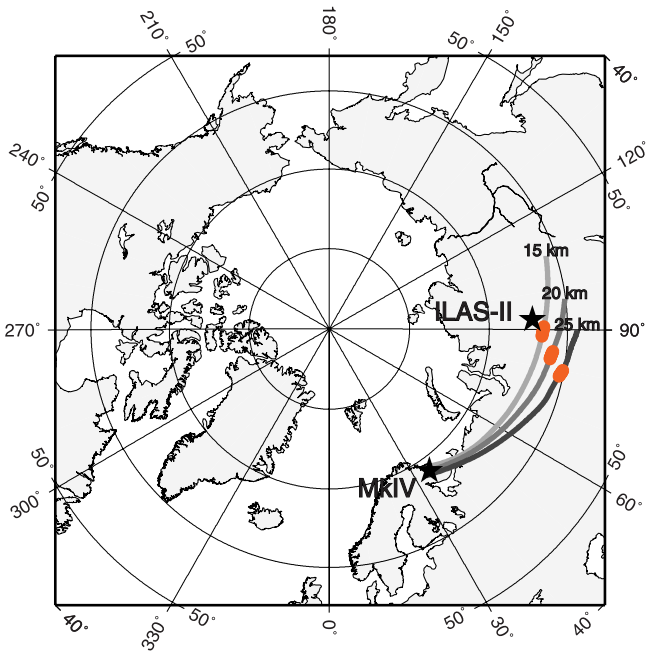

Figure 1. Locations of the MkIV and ILAS-II measurements (stars). These measurements were made on 1 and 2 April 2003, respectively. Two-day isentropic forward trajectories from the MkIV measurement locations at 15, 20, and 25 km are shown with different curves. Red symbols indicate the locations of the trajectories at times within 1 hour of the ILAS-II measurements.

encountered an ILAS-II measurement on 2 April, within a 600-km distance and a 1-hour time difference from the MkIV air mass trajectory at 20 km (Table 4). For the potential temperature level corresponding to the 20-km altitude of the MkIV measurements, the PV difference between the ILAS-II and MkIV measurement times and locations was only 1% (Table 4). These meteorological conditions indicate that the HNO_3 profiles measured by MIPAS-B2 and MkIV should be appropriate for validating the corresponding ILAS-II HNO_3 profiles. To make precise comparisons with MIPAS-B2 and MkIV measurements, the ILAS-II HNO_3 values are linearly interpolated to the potential temperature levels corresponding to the balloon measurement altitudes. In addition, we assume that O_3 is a long-lived tracer in order to carefully search pairs of air masses having the same HNO_3 concentrations. This assumption is valid because little or no chemical ozone loss likely occurred during the short time periods between the ILAS-II and balloon measurements ($<\sim$34 hours (Table 4)). Detailed comparisons are then made only for altitudes where ILAS-II O_3 concentrations agree with those of balloon measurements to within the combined error ranges for ILAS-II and the balloon data.

3.2. Results and Discussion

[11] In Figures 2 and 3, the HNO_3 profiles measured by ILAS-II are compared with those measured by MIPAS-B2 and MkIV, respectively. For each balloon HNO_3 profile, one coincident ILAS-II profile is shown. In Figures 2 and 3, the dotted curves represent the total errors of the ILAS-II HNO_3 data. The horizontal bars show the total errors in HNO_3 (random + systematic errors) for the balloon measurements. As seen in Figure 2a, the HNO_3 mixing ratios derived from ILAS-II measurements agree with the MIPAS-B2 values to within their combined errors at 15–22 and 25–26 km. The relative differences in HNO_3 (Figure 2b), defined as ((ILAS-II data) – (other data))/(other data), are shown with solid symbols for 15–21, 24–28, and 31 km where the difference between O_3 mixing ratios obtained by ILAS-II and MIPAS-B2 was within their combined error ranges. Thirteen comparison pairs selected using O_3 in this way show that the relative differences in HNO_3 range from 0% to +14% at 15–21 km and from +9% to +35% at 24–28 and 31 km (Figure 2b).

[12] For the comparison with MkIV measurements, the ILAS-II HNO_3 mixing ratios agreed with those of MkIV to within the combined errors at 12–13, 15–18, 20–21, and 28–31 km (Figure 3a). Below the altitude of peak HNO_3 mixing ratio, the stratospheric HNO_3 and O_3 mixing ratios generally show a positive correlation, similar to NO_y-O_3 correlations [*Murphy et al.*, 1993; *Fahey et al.*, 1996; *Michelsen et al.*, 1998]. For altitudes below 22 km, where MkIV HNO_3 values are at their maximum, the O_3 mixing ratios derived from the ILAS-II measurements were systematically greater than MkIV O_3 data by 0.3–0.5 ppmv at 14–16 km and lower by 0.3–0.5 ppbv at 19–22 km. These

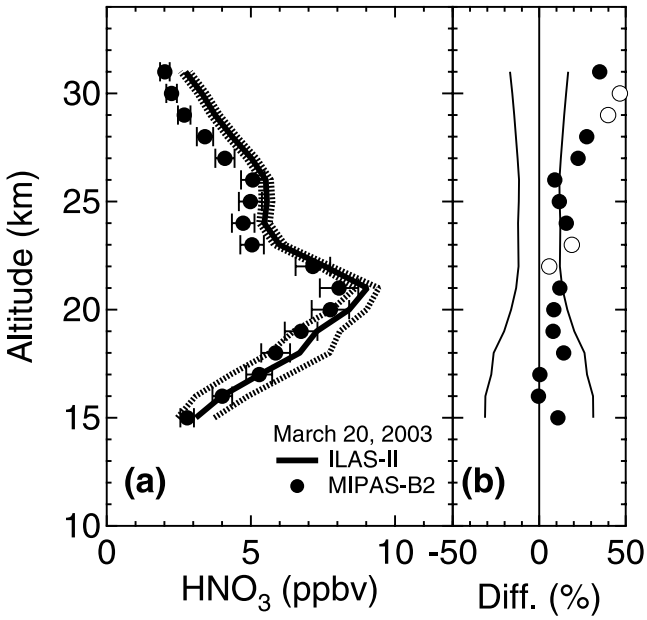

Figure 2. (a) Vertical profiles of HNO_3 mixing ratio measured by ILAS-II and MIPAS-B2 on 20 March 2003 and (b) the relative differences ((ILAS-II value) – (MIPAS-B2 value))/(MIPAS-B2 value). The dotted curves in Figure 2a represent the total errors of the ILAS-II HNO_3 measurements. Total errors of the balloon measurements are shown with error bars. These combined errors are shown with two thin curves in Figure 2b. The relative differences are shown with solid and open symbols when the differences in O_3 between ILAS-II and MIPAS-B2 are within and out of their combined error ranges, respectively.

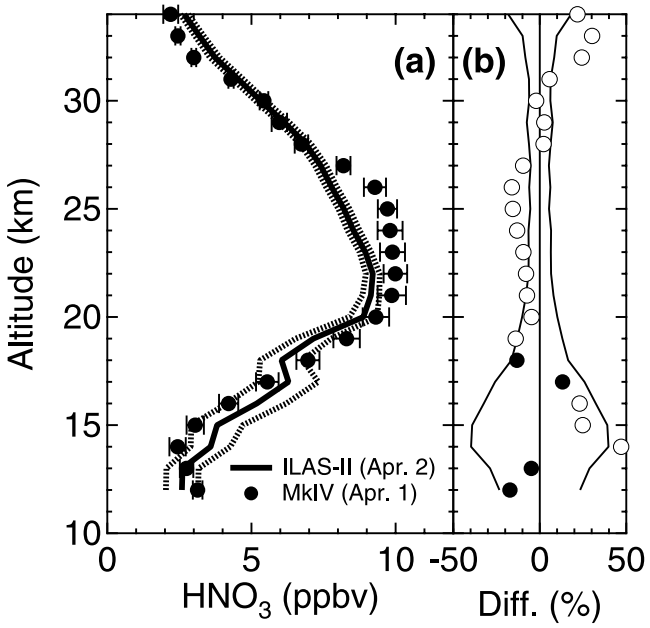

Figure 3. (a and b) Same as Figure 2 but for the comparison of HNO_3 vertical profiles measured by ILAS-II and MkIV on 2 and 1 April 2003, respectively.

differences in O_3 exceeded the combined O_3 error ranges for the ILAS-II and MkIV measurements. Correspondingly, the ILAS-II HNO_3 mixing ratios are greater than the MkIV data by 0.8–1.2 ppbv at 14–16 km and lower by 0.4–1.2 ppbv at 19–22 km (Figure 3a), indicating that O_3 is useful for optimizing HNO_3 comparison conditions in the lower stratosphere. Such significant differences in O_3 were found at 14–16 and 19–33 km, and thus the comparisons for these altitudes are excluded from the following analyses, resulting in only 4 coincident pairs of ILAS-II/MkIV air masses. For these coincident pairs, found at altitudes of 12–13 and 17–18 km, where no significant differences in O_3 occurred, the relative differences in HNO_3 ranged between −17% and +13%, as shown with solid symbols in Figure 3b.

[13] We note here that in the present study the vertical profiles of HNO_3 mixing ratio derived from ILAS-II observations have been compared with only two balloon HNO_3 profiles. It is unlikely that the calculated differences give a quantitative estimate of the accuracy of the ILAS-II HNO_3 measurements, because the number of balloon data available is small and the calculated differences may have uncertainties of at least 15–17%, due to the total errors of the balloon measurements used (Table 4). Therefore we make additional estimates from the standpoint of climatology below, using the HNO_3-O_3 correlations.

4. Climatological Comparison

4.1. Approach

[14] We next compare the ILAS-II HNO_3 data obtained in 2003 with those obtained by ILAS (version 6) in 1997 to further evaluate the ILAS-II HNO_3 data from the standpoint of climatology. As shown in Figures 4 and 5, both the ILAS-II and ILAS observations were made between April and June and covered very similar geographic latitudes and equivalent latitudes (ELs). EL is defined as the geographic latitude enclosing the area where PV values are greater than or equal to a given PV value [*Butchart and Remsberg*, 1986]. Vertical profiles of HNO_3 in 2003 may be different from those in 1997, especially for the seasons when diabatic descent of stratospheric air generally occurs. To minimize the effect of the year-to-year variations in HNO_3 profiles on the climatological ILAS-II/ILAS comparison, we use O_3 as a long-lived tracer for the specific latitudes and seasons where and when the ILAS data show very compact HNO_3-O_3 correlations in 1997. The climatological comparison method using O_3 is described in detail below.

[15] It is well recognized that HNO_3 is the predominant component of the total reactive nitrogen (NO_y) in the mid- and high-latitude lower stratosphere (at ~10–25 km) [*Kawa et al.*, 1992; *Sen et al.*, 1998; *Kondo et al.*, 2000b; *Wetzel et al.*, 2002]. The HNO_3/NO_y ratio varies depending primarily on altitude, season, and aerosol loading [*Mills et al.*, 1993; *Koike et al.*, 1994; *Sen et al.*, 1998]. On the other hand, because of intense production of NO_y and O_3 in the upper tropical stratosphere and their longer lifetimes relative to horizontal mixing [*Plumb and Ko*, 1992], the correlation between NO_y and O_3 mixing ratios are usually compact throughout the lower stratosphere, even at mid and high latitudes [*Murphy et al.*, 1993; *Fahey et al.*, 1996; *Michelsen et al.*, 1998], except inside the polar vortex where severe chemical ozone depletion and denitrification occasionally

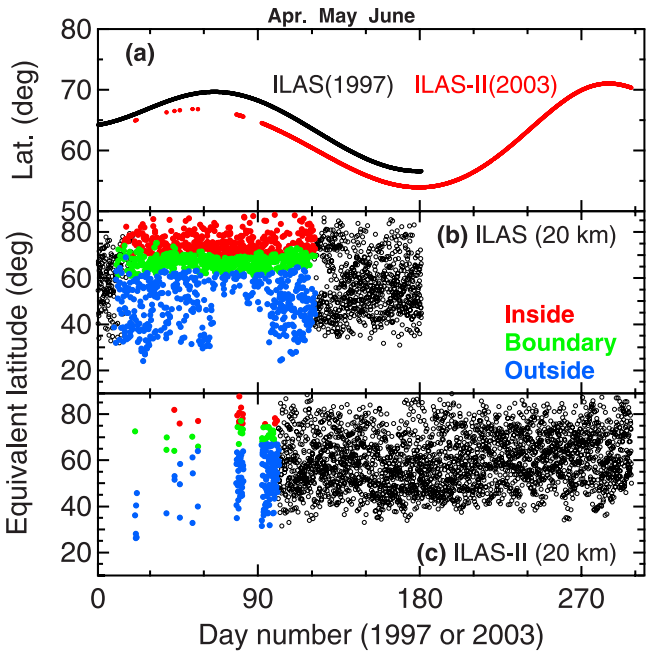

Figure 4. Locations of the measurements made by ILAS and ILAS-II at 20 km for the Northern Hemisphere. (a) Measurement latitudes for ILAS and ILAS-II are shown in black and red, respectively. Equivalent latitudes for (b) ILAS and (c) ILAS-II. The measurements were categorized into regions inside the vortex (red), in the boundary region (green), and outside the vortex (blue), using the method of *Nash et al.* [1996]. The equivalent latitudes are shown in black only for the periods when the polar vortex was much weaker relative to the winter/spring season.

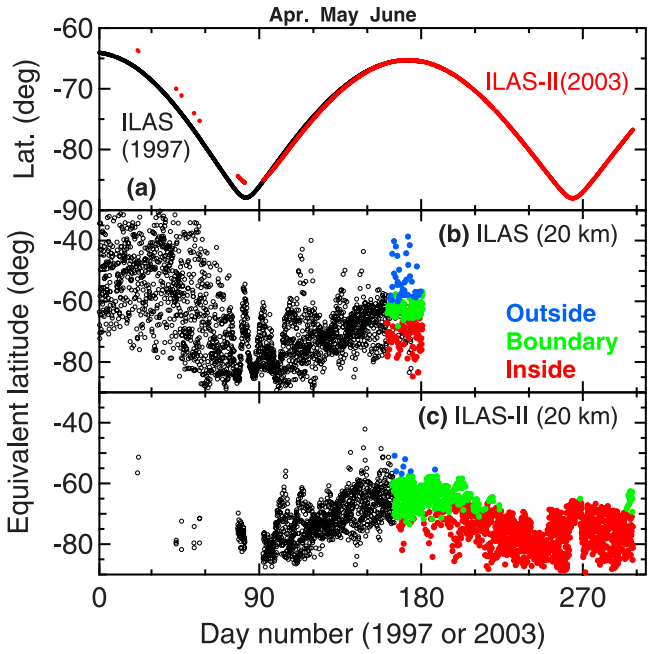

Figure 5. (a–c) Same as Figure 4 but for the Southern Hemisphere.

occur. The observations of these NO_y-O_3 correlations have revealed a slight seasonal dependence in the slope of the correlations, with a large latitudinal dependence, especially in terms of the tropical, midlatitude, and polar vortex regimes. It can thus be expected that the mid- and high-latitude HNO_3-O_3 correlations at altitudes of 10–25 km would usually be tight and the slope of the correlations would be dependent not only on season and aerosol loading but also on EL.

[16] In Figures 4 and 5, the ELs of the ILAS and ILAS-II measurements at 20 km are shown in black only for the periods when the polar vortex was much weaker relative to the winter/spring season. For these periods, the daily maximum of the value (dPV/dEL) × (average wind speed along PV isolines) was less than 30% of the wintertime maximum at potential temperature levels corresponding to about 20 km. Considering the typical seasonal evolution of the polar vortex, the Arctic and Antarctic vortex strengths were least in June and April, respectively, in the months when ILAS-II and ILAS measurements overlapped (April–June). The polar vortex might no longer exist during the overlap months, especially over the Arctic in June. Under these meteorological conditions, little or no chemical ozone depletion or denitrification likely occurred over the Arctic in June or over the Antarctic in April. For June and April, we focus on the HNO_3-O_3 correlations obtained at ELs of 75° ± 5°N and 60° ± 5°S, respectively, because ILAS observed the tightest HNO_3-O_3 correlations at these ELs in 1997. The 1σ HNO_3 standard deviations of the ILAS correlations for the above ELs and seasons were less than ~0.7 ppbv for every 0.5-ppmv O_3 range. The value of 0.7 ppbv is comparable to the precision of the ILAS HNO_3 measurements (~0.8 ppbv [*Koike et al.*, 2000; *Irie et al.*, 2002]).

[17] For ELs of 75° ± 5°N in June and 60° ± 5°S in April, the only factor producing a difference between HNO_3-O_3 correlations in 1997 and 2003 should be aerosol loading, because the correlation depends primarily on season, EL, and aerosol loading, as discussed above. The stratospheric aerosol loading has reached very low levels from the late 1990s to the present because of low volcanic activity, according to the integrated backscatter from the Fraunhofer Institute for Atmospheric Environmental Research lidar and Stratospheric Aerosol and Gas Experiment (SAGE) II measurements [*World Meteorological Organization* (*WMO*), 2003]. Thus the lower stratospheric HNO_3-O_3 correlations at ELs of 75° ± 5°N in June 1997 and at ELs of 60° ± 5°S in April 1997 should most likely be similar to those for 2003, and therefore the HNO_3 measurements made by ILAS-II can be evaluated by comparing the HNO_3-O_3 correlations obtained by ILAS-II and ILAS for these EL ranges and seasons. To confirm that the HNO_3-O_3 correlations at those ELs and seasons are invariant over a timescale of years, we also analyze the UARS/MLS HNO_3 (version 6) and O_3 data (version 5) [*Santee et al.*, 2004]. To perform a quantitative evaluation as a function of altitude, we compare HNO_3 mixing ratios measured by ILAS-II with the reference HNO_3 (referred to as HNO^*_3) values, which are calculated from the O_3 mixing ratios measured by ILAS-II using the tight correlations between HNO_3 and O_3 observed by ILAS. All of the mixing ratios required in this calculation and the following analyses have been scaled according to their estimated bias (for NH at 20 km, for example, +2% for ILAS HNO_3 [*Irie et al.*, 2002], +3% for ILAS O_3

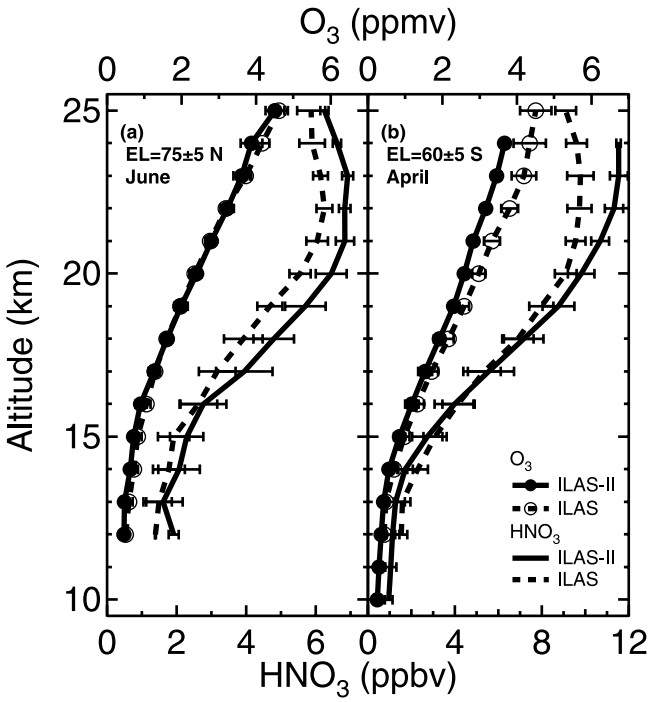

Figure 6. Mean vertical profiles of HNO_3 and O_3 obtained (a) at ELs = 75° ± 5°N in June and (b) at ELs = 60° ± 5°S in April. HNO_3 and O_3 profiles are indicated by lines without and with symbols, respectively. Solid and dashed lines indicate data obtained by ILAS-II in 2003 and by ILAS in 1997, respectively. One-σ standard deviations are shown with error bars.

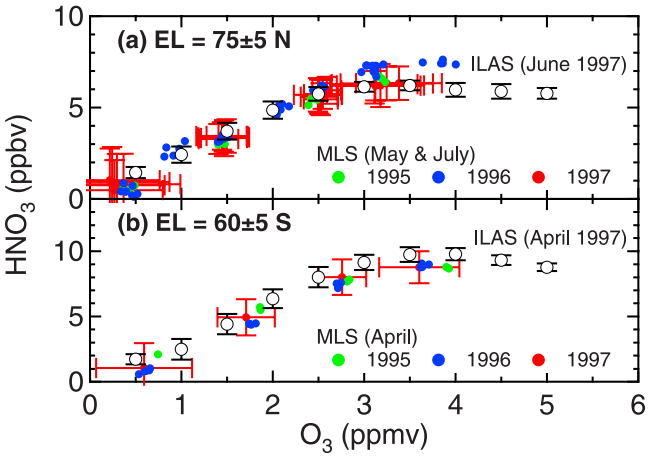

Figure 7. HNO_3-O_3 correlations obtained by ILAS (open symbols) and MLS (solid symbols) at (a) ELs = 75° ± 5°N and (b) ELs = 60° ± 5°S. Time periods during which the data were obtained are described. For ILAS, the averages of the HNO_3 mixing ratios for each 0.5-ppmv O_3 range are plotted. One-σ standard deviations are shown with error bars. For MLS, correlations between daily averaged HNO_3 and O_3 mixing ratios measured at each of four potential temperature levels between 420 K (∼17 km) and 585 K (∼24 km) are shown. Measurements made in 1995, 1996, and 1997 are shown in green, blue, and red, respectively. One-σ standard deviations of HNO_3 and O_3 data are shown only for 1997, for clarity.

[*Sugita et al.*, 2002], and −2% for ILAS-II O_3 [*Sugita et al.*, 2006].

4.2. Results and Discussion

[18] In Figure 6a, mean vertical profiles of HNO_3 and O_3 mixing ratios observed by ILAS-II at ELs of 75° ± 5°N in June 2003 are compared with those observed by ILAS in 1997. For all the altitudes between 12 and 25 km, ILAS-II O_3 mixing ratios agree with those of ILAS to within their standard deviations. However, for ELs of 60° ± 5°S in April, when diabatic descent of stratospheric air generally occurs especially at higher altitudes, the comparison between O_3 profiles observed by ILAS-II and ILAS show larger differences at higher altitudes (Figure 6b). The differences are presumably due to a difference in diabatic descent between 2002 and 1997. To reduce such an effect on the comparison of HNO_3 profiles measured by ILAS-II and ILAS, we use HNO_3-O_3 correlations below.

[19] For ELs of 75° ± 5°N in June 1997 and ELs of 60° ± 5°S in April 1997, the HNO_3-O_3 correlations obtained by ILAS are shown with open symbols in Figures 7a and 7b, respectively. The mean and 1σ standard deviations of ILAS HNO_3 values in each 0.5-ppmv O_3 range are shown. The numbers of data points used for each 0.5-ppmv O_3 range are 22–62 and 35–147 for ELs of 75° ± 5°N and 60° ± 5°S, respectively. The ILAS HNO_3 values plotted in Figures 7a and 7b are the predefined HNO_3 values as a function of O_3 mixing ratio.

[20] Long-term, simultaneous measurements of stratospheric HNO_3 and O_3 mixing ratios were made by UARS/MLS from 1991 through 2000. In Figures 7a and 7b, the correlations between the daily averages of the HNO_3 and O_3 mixing ratios derived from the MLS observations are also shown for ELs of 75° ± 5°N in May and July and for 60° ± 5°S in April, respectively. Averages of the MLS data were calculated for each of four different potential temperature levels, namely 420 K (∼17 km), 465 K (∼19 km), 525 K (∼22 km), and 585 K (∼24 km). It should be noted that for ELs of 75° ± 5°N we plotted the MLS data for May and July, instead of June, because MLS seldom or never made measurements in the NH in June [*Santee et al.*, 2004]. We also note that Figures 7a and 7b show the HNO_3-O_3 correlations only for 1995–1997, because variations in stratospheric aerosol loading [*WMO*, 2003] could affect the correlations in 1991–1994, and the MLS measurements in 1998–2000 were much more sparse relative to 1995–1997 [*Santee et al.*, 2004].

[21] Considering that the precision of the individual HNO_3 profile measurements by MLS is as good as 1.0–1.5 ppbv [*Santee et al.*, 2004], larger error bars on the MLS HNO_3-O_3 correlations relative to those for ILAS (Figure 7) can be attributed to the poorer vertical resolution of the MLS measurements (5–10 km) compared to that of the ILAS measurements (1.9–3.5 km), because HNO_3 and O_3 mixing ratios vary with altitude. As seen in Figure 7, the differences in MLS HNO_3 mixing ratios among the different years 1995–1997 are all less than 1.5 ppbv at the same O_3 mixing ratio. This indicates that the lower stratospheric HNO_3-O_3 correlations were almost invariant over years 1995–1997 for the above ELs and seasons. The results support the assumption made in the present study that the lower stratospheric HNO_3-O_3 correlations were invariant for these ELs and seasons over several years. Furthermore, the ILAS HNO_3-O_3 correlations agree well with those of MLS in 1997 for these ELs and seasons, confirming that the ILAS correlations are suitable for making climatological comparisons with ILAS-II HNO_3 data.

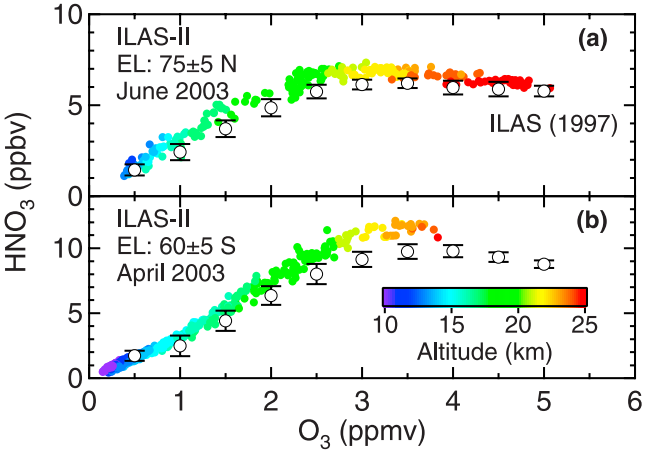

Figure 8. HNO_3-O_3 correlations obtained by ILAS-II (a) at ELs = 75° ± 5°N in June 2003 and (b) at ELs = 60° ± 5°S in April 2003. The correlations are shown with solid symbols. Colors indicate the altitudes of the measurements. For comparison, the correlations obtained by ILAS in 1997 at the same ELs and seasons are also shown with open symbols.

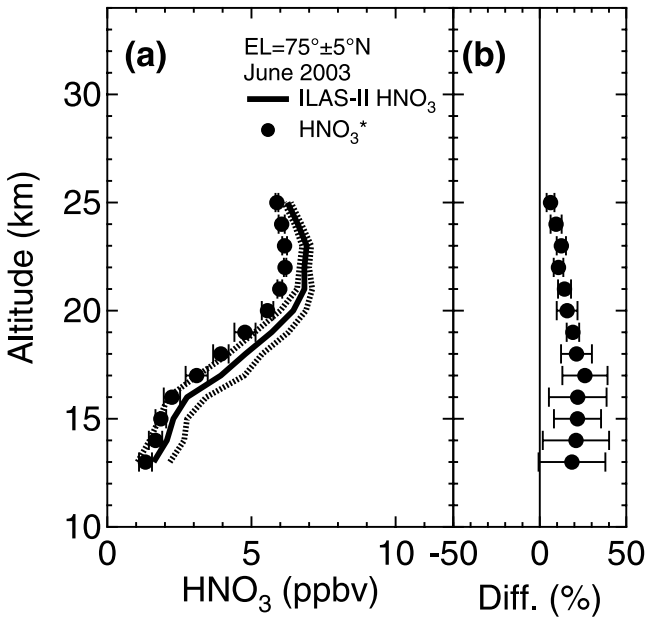

Figure 9. (a) Vertical profiles of ILAS-II HNO_3 values (line) and reference HNO_3 (HNO^*_3) values (symbols) for ELs = 75° ± 5°N in June. The associated dotted curves and error bars represent 1σ standard deviations for ILAS-II HNO_3 and HNO^*_3, respectively. (b) Vertical profile of the mean relative differences between the ILAS-II HNO_3 and HNO^*_3 values is shown. Error bars represent 1σ standard deviations.

[22] In Figures 8a and 8b, the HNO_3-O_3 correlations obtained by ILAS-II (solid symbols) are plotted together with those of ILAS (open symbols), for ELs of 75° ± 5°N in June and for ELs of 60° ± 5°S in April, respectively. It can be readily seen from Figures 8a and 8b that the HNO_3-O_3 correlations measured by ILAS-II were compact, as well as those measured by ILAS. However, the ILAS-II correlations systematically depart from ILAS correlations, especially at higher altitudes for ELs of 60° ± 5°S in April (Figure 8b). Similar systematic differences are also seen from the comparison with MLS data; while the daily averages of HNO_3 mixing ratios obtained by MLS in 1995–1997 were all less than ~10 ppbv (Figure 7b), the ILAS-II HNO_3 values reached ~11.5 ppbv (Figure 8b) and were systematically greater than the MLS values when we consider the precision of the MLS measurements (1.0–1.5 ppbv).

[23] To make quantitative estimates of the difference as a function of altitude, the mean HNO_3 vertical profile measured by ILAS-II at ELs of 75° ± 5°N in June is compared with the mean profile of HNO^*_3 values, which were calculated from ILAS HNO_3-O_3 correlations and ILAS-II O_3 data. In Figure 9a, the dotted curves and error bars represent the 1σ standard deviations of the ILAS-II HNO_3 and HNO^*_3 values, respectively. The mean relative differences between ILAS-II HNO_3 and HNO^*_3 values ranged from +9 to +26% at 13–25 km (Figure 9b). Similarly, in the comparison at ELs of 60° ± 5°S in April, ILAS-II HNO_3 values are systematically greater than HNO^*_3 by 17–24% at 15–24 km (Figure 10b). These results suggest that the ILAS-II HNO_3 data could have some positive biases at 15–25 km altitude, although the exact magnitude of the bias cannot be quantified only from these comparisons because the results are fully based on climatological comparisons.

[24] The standard deviations of the relative differences between the ILAS-II HNO_3 and HNO^*_3 values are shown with error bars in Figures 9b and 10b. These standard deviations are the result of the scatter of the ILAS-II HNO_3 values around the HNO^*_3 values. The HNO^*_3 values were calculated from O_3, the spatial distribution of which was most likely controlled mainly by dynamical processes for the altitudes, latitudes, and seasons used in the present study. The use of HNO^*_3 values thus accounts for some dynamical effects on the HNO_3 spatial distribution, so that these effects are considered to be reduced in the above calculations of the standard deviations. Therefore it is expected that the standard deviations of the differences between the ILAS-II HNO_3 and HNO^*_3 values give an upper limit of the precision of the ILAS-II HNO_3 measurements.

[25] For the ILAS-II measurements made in NH in June (in SH in April), the standard deviations of the differences between the ILAS-II HNO_3 and HNO^*_3 values were estimated to be 14% (13%), 6% (6%), and 2% (1%) at 15, 20, and 25 km, respectively, as shown in Figure 9b (10b). We have used repeatability errors to derive upper limits of the precision of the ILAS-II HNO_3 measurements, as described above. The derived precision for the NH (SH) measurements were 23% (17%), 5% (5%), and 1% (3%) at 15, 20, and 25 km, respectively (Table 1), and were very similar to those calculated from the standard deviations. These results indicate that the spatial inhomogeneity of HNO_3 can be substantially reduced by using HNO^*_3 at the measurement times and locations for which O_3 can be regarded as a long-lived tracer. Considering that both of the estimates give upper limit values, the precision of the ILAS-II HNO_3 measurements for NH (SH) is estimated to be better than

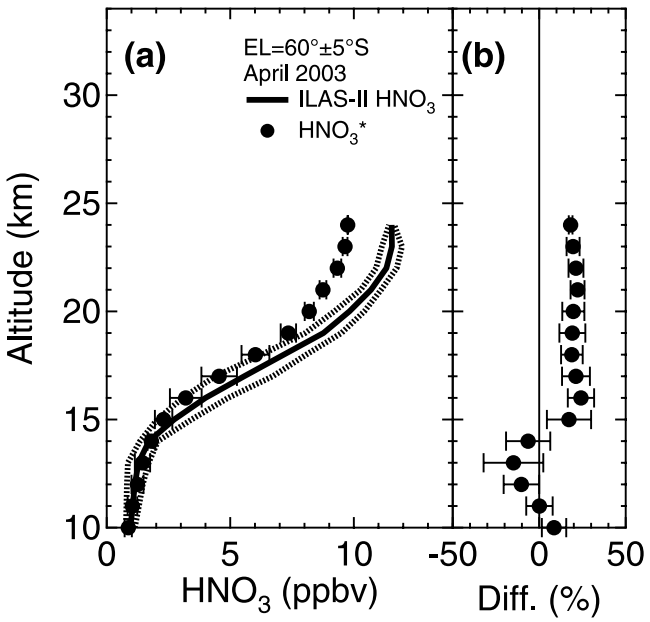

Figure 10. (a and b) Same as Figure 9 but for ELs = 60° ± 5°S in April.

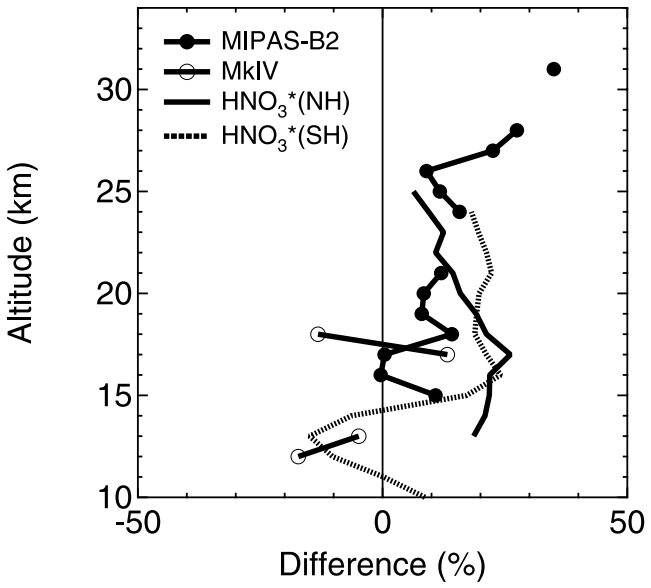

Figure 11. Vertical profiles of the relative differences of ILAS-II HNO_3 mixing ratios with those measured by MIPAS-B2 (solid circles) and MkIV (open circles) and HNO_3^* values for NH (ELs = 75° ± 5°N) in June (solid line) and for SH (ELs = 60° ± 5°S) in April (dotted line).

14% (13%), 5% (5%), and 1% (1%) at 15, 20, and 25 km, respectively.

[26] Figure 11 summarizes the results from all the comparisons of HNO_3 profiles derived from ILAS-II observations with those derived from balloon observations and the HNO_3^* values. At 15–25 km, where comparisons are more robust than at other altitudes, the maximum and minimum of the relative differences of the ILAS-II HNO_3 data from balloon or HNO_3^* values reached −13% and +26%, respectively (Figure 11). Since this range of relative differences cannot be explained only by the above estimates of the precision of the ILAS-II HNO_3 measurements and errors in the data compared with ILAS-II data, part of the differences should reflect the accuracy of the ILAS-II measurements. Using the maximum and minimum of the difference, the accuracy of the ILAS-II HNO_3 measurements at 15–25 km is estimated to be better than −13%/+26%. The most plausible magnitude of the bias in ILAS-II HNO_3 data at 15–25 km is +14%, which is the average of all the differences given at 15–25 km. Because the wintertime variations of the HNO_3 concentration at these altitudes in the Antarctic vortex are generally much larger than the estimated precision and accuracy of HNO_3 measurements by ILAS-II [e.g., *Santee et al.*, 2004], the ILAS-II HNO_3 data would be useful for investigating the processes leading to PSC formation and denitrification, as well as the spatial distribution and temporal variation of HNO_3.

5. Conclusions

[27] We have compared vertical profiles of ILAS-II HNO_3 data (version 1.4) with those obtained by balloon-borne instruments (MIPAS-B2 and MkIV) over the Arctic in March and April 2003 to assess the validity of the ILAS-II HNO_3 data. Additional assessments were made by comparing ILAS-II HNO_3 data with HNO_3^* values for ELs = 75° ± 5°N in June 1997 and for ELs = 60° ± 5°S in April 1997, where HNO_3^* was calculated from the O_3 mixing ratios measured by ILAS-II using the ILAS HNO_3-O_3 correlations that were likely maintained from 1997 until 2003 for these ELs and seasons. In support of this assumption, UARS/MLS data showed that the lower stratospheric HNO_3-O_3 correlations for these ELs and seasons were very compact and almost invariant over several years between 1995 and 1997.

[28] For the lower stratosphere, the standard deviation of the differences between the ILAS-II HNO_3 and HNO_3^* values provided a good quantitative estimate of the precision of the ILAS-II HNO_3 mixing ratio data. This is because the spatial inhomogeneity of HNO_3 mixing ratios at a given altitude in the lower stratosphere is largely reduced by using HNO_3^* as a reference. Using this technique, the precision of the HNO_3 measurements by ILAS-II at 15, 20, and 25 km was estimated to be better than 13–14%, 5%, and 1%, respectively.

[29] For all of the comparisons with balloon data and HNO_3^* values, differences in HNO_3, defined as ((ILAS-II data) – (other data))/(other data), ranged between −13% and +26% at 15–25 km. This indicates that the accuracy of the ILAS-II HNO_3 data is better than −13%/+26% at 15–25 km. The ILAS-II HNO_3 values tended to be systematically greater than balloon data and HNO_3^* values. The most plausible bias in the ILAS-II HNO_3 data is +14% at 15–25 km. The results presented here thus provide the quantitative basis for investigating polar stratospheric chemistry and dynamics using ILAS-II HNO_3 data.

[30] **Acknowledgments.** The authors are grateful to all the members of the ILAS-II science team for their contributions to the ILAS-II project. We also thank the Fujitsu FIP Corporation for processing the ILAS-II data at the Data Handling Facility (DHF) of the National Institute for Environmental Studies (NIES). Support from the Ministry of the Environment is gratefully acknowledged. Part of this work was carried out when H.I. was at NIES. Work at the Jet Propulsion Laboratory, California Institute of Technology, was done under contract with NASA.

References

Butchart, N., and E. E. Remsberg (1986), The area of the stratospheric polar vortex as a diagnostic for tracer transport on an isentropic surface, *J. Atmos. Sci.*, *43*, 1319–1339.

Fahey, D. W., et al. (1996), In situ observations of NO_y, O_3, and the NO_y/O_3 ratio in the lower stratosphere, *Geophys. Res. Lett.*, *23*(13), 1653–1656.

Friedl-Vallon, F., G. Maucher, A. Kleinert, A. Lengel, C. Keim, H. Oelhaf, H. Fischer, M. Seefeldner, and O. Trieschmann (2004), Design and characterization of the balloon-borne Michelson Interferometer for Passive Atmospheric Sounding, *Appl. Opt.*, *43*, 3335–3355.

Hayashida, S., N. Saitoh, A. Kagawa, T. Yokota, M. Suzuki, H. Nakajima, and Y. Sasano (2000), Arctic polar stratospheric clouds observed with the Improved Limb Atmospheric Spectrometer during winter 1996/1997, *J. Geophys. Res.*, *105*(D20), 24,715–24,730.

Irie, H., and Y. Kondo (2003), Evidence for the nucleation of polar stratospheric clouds inside liquid particles, *Geophys. Res. Lett.*, *30*(4), 1189, doi:10.1029/2002GL016493.

Irie, H., M. Koike, Y. Kondo, G. E. Bodeker, M. Y. Danilin, and Y. Sasano (2001), Redistribution of nitric acid in the Arctic lower stratosphere during the winter of 1996–1997, *J. Geophys. Res.*, *106*(D19), 23,139–23,150.

Irie, H., et al. (2002), Validation of NO_2 and HNO_3 measurements from the Improved Limb Atmospheric Spectrometer (ILAS) with the version 5.20 retrieval algorithm, *J. Geophys. Res.*, *107*(D24), 8206, doi:10.1029/2001JD001304.

Irie, H., K. L. Pagan, A. Tabazadeh, M. J. Legg, and T. Sugita (2004), Investigation of polar stratospheric cloud solid particle formation

mechanisms using ILAS and AVHRR observations in the Arctic, *Geophys. Res. Lett.*, *31*, L15107, doi:10.1029/2004GL020246.

Kawa, S. R., D. W. Fahey, L. E. Heidt, W. H. Pollock, S. Solomon, D. E. Anderson, M. Loewenstein, M. H. Proffitt, J. J. Margitan, and K. R. Chan (1992), Photochemical partitioning of the reactive nitrogen and chlorine reservoirs in the high-latitude stratosphere, *J. Geophys. Res.*, *97*(D8), 7905–7923.

Koike, M., N. B. Jones, W. A. Matthews, P. V. Johnston, R. L. McKenzie, D. Kinnison, and J. Rodriguez (1994), Impact of Pinatubo aerosols on the partitioning between NO_2 and HNO_3, *Geophys. Res. Lett.*, *21*(7), 597–600.

Koike, M., et al. (2000), A comparison of Arctic HNO_3 profiles measured by the Improved Limb Atmospheric Spectrometer and balloon-borne sensors, *J. Geophys. Res.*, *105*(D5), 6761–6771.

Kondo, Y., H. Irie, M. Koike, and G. E. Bodeker (2000a), Denitrification and nitrification in the Arctic stratosphere during the winter of 1996–1997, *Geophys. Res. Lett.*, *27*(3), 337–340.

Kondo, Y., T. Sugita, M. Koike, S. R. Kawa, M. Y. Danilin, J. M. Rodriguez, S. Spreng, K. Golinger, and F. Arnold (2000b), Partitioning of reactive nitrogen in the midlatitude lower stratosphere, *J. Geophys. Res.*, *105*(D1), 1417–1424.

Michelsen, H. A., G. L. Manney, M. R. Gunson, and R. Zander (1998), Correlations of stratospheric abundances of NO_y, O_3, N_2O, and CH_4 derived from ATMOS measurements, *J. Geophys. Res.*, *103*(D21), 28,347–28,359.

Mills, M. J., A. O. Langford, T. J. O'Leary, K. Arpag, H. L. Miller, M. H. Proffitt, R. W. Sanders, and S. Solomon (1993), On the relationship between stratospheric aerosols and nitrogen dioxide, *Geophys. Res. Lett.*, *20*(12), 1187–1190.

Murphy, D. M., D. W. Fahey, M. H. Proffitt, S. C. Liu, K. R. Chan, C. S. Eubank, S. R. Kawa, and K. K. Kelly (1993), Reactive nitrogen and its correlation with ozone in the lower stratosphere and upper troposphere, *J. Geophys. Res.*, *98*(D5), 8751–8773.

Nakajima, H., et al. (2002), Tangent height registration for the solar occultation satellite sensor ILAS: A new technique for version 5.20 products, *J. Geophys. Res.*, *107*(D24), 8215, doi:10.1029/2001JD000607.

Nash, E. R., P. A. Newman, J. E. Rosenfield, and M. R. Schoeberl (1996), An objective determination of the polar vortex using Ertel's potential vorticity, *J. Geophys. Res.*, *101*(D5), 9471–9478.

Oelhaf, H., et al. (1996), Remote sensing of the Arctic stratosphere with the new balloon-borne MIPAS-B2 instrument, in *Proceedings of the 3rd European Workshop*, edited by J. A. Pyle, N. R. P. Harris, and G. T. Amanatidis, pp. 270–275, Eur. Comm., Brussels.

Plumb, R. A., and M. K. W. Ko (1992), Interrelationships between mixing ratios of long-lived stratospheric constituents, *J. Geophys. Res.*, *97*(D9), 10,145–10,156.

Rivière, E. D., Y. Terao, and H. Nakajima (2003), A Lagrangian method to study stratospheric nitric acid variations in the polar regions as measured by the Improved Limb Atmospheric Spectrometer, *J. Geophys. Res.*, *108*(D23), 4718, doi:10.1029/2003JD003718.

Rothman, L. S., et al. (2003), The HITRAN molecular spectroscopic database: Edition of 2000 including updates through 2001, *J. Quant. Spectrosc. Radiat. Transfer*, *82*, 5–44.

Saitoh, N., S. Hayashida, Y. Sasano, and L. L. Pan (2002), Characteristics of Arctic polar stratospheric clouds in the winter of 1996/1997 inferred from ILAS measurements, *J. Geophys. Res.*, *107*(D24), 8205, doi:10.1029/2001JD000595.

Santee, M. L., W. G. Read, J. W. Waters, L. Froidevaux, G. L. Manney, D. A. Flower, R. F. Jarnot, R. S. Harwood, and G. E. Peckham (1995), Interhemispheric differences in polar stratospheric HNO_3, H_2O, ClO, and O_3, *Science*, *267*, 849–852.

Santee, M. L., G. L. Manney, L. Froidevaux, R. W. Zurek, and J. W. Waters (1997), MLS observations of ClO and HNO_3 in the 1996–97 Arctic polar vortex, *Geophys. Res. Lett.*, *24*(22), 2713–2716.

Santee, M. L., A. Tabazadeh, G. L. Manney, R. J. Salawitch, L. Froidevaux, W. G. Read, and J. W. Waters (1998), UARS Microwave Limb Sounder HNO_3 observations: Implications for Antarctic polar stratospheric clouds, *J. Geophys. Res.*, *103*(D11), 13,285–13,313.

Santee, M. L., G. L. Manney, L. Froidevaux, W. G. Read, and J. W. Waters (1999), Six years of UARS Microwave Limb Sounder HNO_3 observations: Seasonal, interhemispheric, and interannual variations in the lower stratosphere, *J. Geophys. Res.*, *104*(D7), 8225–8246.

Santee, M. L., G. L. Manney, N. J. Livesey, and J. W. Waters (2000), UARS Microwave Limb Sounder observations of denitrification and ozone loss in the 2000 Arctic late winter, *Geophys. Res. Lett.*, *27*(19), 3213–3216.

Santee, M. L., A. Tabazadeh, G. L. Manney, M. D. Fromm, R. M. Bevilacqua, J. W. Waters, and E. J. Jensen (2002), A Lagrangian approach to studying Arctic polar stratospheric clouds using UARS MLS HNO_3 and POAM II aerosol extinction measurements, *J. Geophys. Res.*, *107*(D10), 4098, doi:10.1029/2000JD000227.

Santee, M. L., G. L. Manney, N. J. Livesey, and W. G. Read (2004), Three-dimensional structure and evolution of stratospheric HNO_3 based on UARS Microwave Limb Sounder measurements, *J. Geophys. Res.*, *109*, D15306, doi:10.1029/2004JD004578.

Sasano, Y., M. Suzuki, T. Yokota, and H. Kanzawa (1999), Improved Limb Atmospheric Spectrometer (ILAS) for stratospheric ozone layer measurements by solar occultation technique, *Geophys. Res. Lett.*, *26*(2), 197–200.

Sen, B., G. C. Toon, G. B. Osterman, J. F. Blavier, J. J. Margitan, R. J. Salawitch, and G. K. Yue (1998), Measurements of reactive nitrogen in the stratosphere, *J. Geophys. Res.*, *103*(D3), 3571–3585.

Sugita, T., et al. (2002), Validation of ozone measurements from the Improved Limb Atmospheric Spectrometer, *J. Geophys. Res.*, *107*(D24), 8212, doi:10.1029/2001JD000602.

Sugita, T., et al. (2006), Ozone profiles in the high-latitude stratosphere and lower mesosphere measured by the Improved Limb Atmospheric Spectrometer (ILAS)-II: Comparison with other satellite sensors and ozonesondes, *J. Geophys. Res.*, doi:10.1029/2005JD006439, in press.

Toon, G. C. (1991), The JPL MkIV interferometer, *Opt. Photonic News*, *2*, 19–21.

Wetzel, G., et al. (2002), NO_y partitioning and budget and its correlation with N_2O in the Arctic vortex and in summer midlatitudes in 1997, *J. Geophys. Res.*, *107*(D16), 4280, doi:10.1029/2001JD000916.

World Meteorological Organization (2003), Scientific assessment of ozone depletion: 2002, *Global Ozone Res. and Monit. Proj., Rep. 47*, 498 pp., Geneva, Switzerland.

Yokota, T., H. Nakajima, T. Sugita, H. Tsubaki, Y. Ito, M. Kaji, M. Suzuki, H. Kanzawa, J. H. Park, and Y. Sasano (2002), Improved Limb Atmospheric Spectrometer (ILAS) data retrieval algorithm for version 5.20 gas profile products, *J. Geophys. Res.*, *107*(D24), 8216, doi:10.1029/2001JD000628.

M. K. Ejiri, H. Nakajima, N. Saitoh, Y. Sasano, T. Sugita, T. Tanaka, and T. Yokota, National Institute for Environmental Studies, 16-2, Onogawa, Tsukuba, Ibaraki 305-8506, Japan.

H. Irie, Frontier Research Center for Global Change, Japan Agency for Marine-Earth Science and Technology, 3173-25 Showa-machi, Kanazawa-ku, Yokohama, Kanagawa 236-0001, Japan. (irie@jamstec.go.jp)

H. Kanzawa, Department of Earth and Environmental Sciences, Graduate School of Environmental Studies, Nagoya University, Furo-cho, Chikusa-ku, Nagoya, Aichi 464-8601, Japan.

H. Kobayashi, Central Research Institute of Electric Power Industry, 1-6-1, Ohtemachi, Chiyoda-ku, Tokyo 100-8126, Japan.

Y. Kondo, Research Center for Advanced Science and Technology, University of Tokyo, Meguro-ku, Tokyo 153-8904, Japan.

H. Oelhaf and G. Wetzel, Institut für Meteorologie und Klimaforschung, Forschungszentrum Karlsruhe, P.O. Box 3640, D-76021 Karlsruhe, Germany.

M. L. Santee, B. Sen, and G. C. Toon, Jet Propulsion Laboratory, California Institute of Technology, 4800 Oak Grove Drive, Pasadena, CA 91109, USA.

Y. Terao, Division of Engineering and Applied Sciences, Harvard University, 29 Oxford Street, Cambridge, MA 02138, USA.